Received: 30 May 2018 | Revised: 26 July 2019 | Accepted: 29 July 2019

DOI: 10.1111/epi.16316

Epilepsia®

FULL-LENGTH ORIGINAL RESEARCH

Both gain-of-function and loss-of-function *de novo CACNA1A* mutations cause severe developmental epileptic encephalopathies in the spectrum of Lennox-Gastaut syndrome

Xiao Jiang[1,2] | **Praveen K. Raju**[1,2] | **Nazzareno D'Avanzo**[3] | **Mathieu Lachance**[1] | **Julie Pepin**[2] | **François Dubeau**[4] | **Wendy G. Mitchell**[5] | **Luis E. Bello-Espinosa**[6] | **Tyler M. Pierson**[7] | **Berge A. Minassian**[8] | **Jean-Claude Lacaille**[2] | **Elsa Rossignol**[1,2]

[1]Sainte-Justine University Hospital Center, University of Montréal, Montréal, Canada

[2]Department of Neurosciences, University of Montréal, Montreal, Canada

[3]Department of Pharmacology and Physiology, University of Montréal, Montréal, Canada

[4]Department of Neurosciences, The Montreal Neurological Institute, McGill University, Montréal, Canada

[5]Neurology Division, Children's Hospital Los Angeles & Department of Neurology, Keck School of Medicine of University of Southern California, Los Angeles, CA, USA

[6]Department of Clinical Neurosciences, University of Calgary, Alberta, Canada

[7]Departments of Pediatrics and Neurology, The Board of Governors Regenerative Medicine Institute, Los Angeles, CA, USA

[8]The Hospital for Sick Children Research Institute, Toronto, Canada

Correspondence
Elsa Rossignol, Sainte-Justine University Hospital Center, University of Montréal, Montréal, Canada.
Email: elsa.rossignol@umontreal.ca

Funding information
Canadian Institutes of Health Research, Grant/Award Number: 10848, 119553 and 125985; Réseau de Médecine Génétique Appliquée (RMGA); Fonds de la Recherche du Québec en Santé (FRQS); Savoy Foundation

Abstract

Objective: Developmental epileptic encephalopathies (DEEs) are genetically heterogeneous severe childhood-onset epilepsies with developmental delay or cognitive deficits. In this study, we explored the pathogenic mechanisms of DEE-associated *de novo* mutations in the *CACNA1A* gene.

Methods: We studied the functional impact of four *de novo* DEE-associated *CACNA1A* mutations, including the previously described p.A713T variant and three novel variants (p.V1396M, p.G230V, and p.I1357S). Mutant cDNAs were expressed in HEK293 cells, and whole-cell voltage-clamp recordings were conducted to test the impacts on $Ca_V2.1$ channel function. Channel localization and structure were assessed with immunofluorescence microscopy and three-dimensional (3D) modeling.

Results: We find that the G230V and I1357S mutations result in loss-of-function effects with reduced whole-cell current densities and decreased channel expression at the cell membrane. By contrast, the A713T and V1396M variants resulted in gain-of-function effects with increased whole-cell currents and facilitated current activation (hyperpolarized shift). The A713T variant also resulted in slower current decay. 3D modeling predicts conformational changes favoring channel opening for A713T and V1396M.

Jiang and Raju contributed equally to the work. Lacaille and Rossignol contributed equally.

Significance: Our findings suggest that both gain-of-function and loss-of-function *CACNA1A* mutations are associated with similarly severe DEEs and that functional validation is required to clarify the underlying molecular mechanisms and to guide therapies.

KEYWORDS

CACNA1A, $Ca_V2.1$, *de novo* mutations, epilepsy, epileptic encephalopathies, immunofluorescence, Lennox-Gastaut syndrome, patch-clamp, structural modeling

1 | INTRODUCTION

Developmental epileptic encephalopathies (DEEs) are a diverse group of severe early onset epilepsies with refractory seizures, developmental delay (DD), and/or intellectual disability (ID) resulting in long-term morbidity and increased mortality.[1–3] The underlying causes of DEEs are heterogeneous and include brain malformations; pre- and perinatal brain lesions (infections, strokes), neurometabolic disorders, chromosomal rearrangements, and various monogenic disorders.

The advent of next-generation sequencing (NGS) methods, including whole exome and genome sequencing, has significantly increased our ability to identify a genetic cause for patients with unexplained nonlesional DEEs, resulting in the identification of a molecular mechanism in approximately 35%-40% of patients.[4–9] DEEs are genetically heterogeneous, with at least 110 genes associated with DEE or with isolated intellectual deficiency.[5] In addition, most DEE-associated mutations are sporadic *de novo* variants rather than inherited dominant or recessive variants as seen in other neurodevelopmental disorders.[5,6] Thus a novel *de novo* variant in a known DEE gene identified in a child with a consistent phenotype is considered likely pathogenic when it is rare and never reported in controls; when it affects highly conserved residues with predicted pathological impact on protein structure, conformation, or function (as predicted by bioinformatics tools); and when it involves a gene that is intolerant to haploinsufficiency.[5] The functional validation to study the direct impact of a given variant on protein localization and function provides more definitive evidence of the variant's pathogenicity and confirms the genetic diagnosis. It also informs on the pathophysiological mechanisms and guides therapies.

We recently reported that inherited dominant loss-of-function (LOF) mutations (ie, deletions or nonsense mutations) in the *CACNA1A* gene, encoding the $\alpha 1_A$-subunit of $Ca_V2.1$ calcium channels, cause DEE with generalized epilepsy, a spectrum of neurocognitive deficits (attention deficit, learning disability, autism spectrum disorder and/or frank intellectual disability [ID]), and a mild form of episodic ataxia.[10] Subsequently, we identified *de novo* variants in the *CACNA1A* gene, including the previously reported A713T variant[7,11] and the novel V1396M variant, in patients with severe DEE in the spectrum of Lennox-Gastaut syndrome (LGS), with refractory generalized seizures (absences, tonic, tonic-clonic, and atonic seizures), moderate-severe ID, and ataxia.[5] We subsequently identified two other *de novo* variants (G230V and I1357S) in an expanded cohort of children with similar phenotypes. In parallel, *de novo* missense *CACNA1A* variants were reported recently in six patients with LGS and/or DEE with developmental ataxia.[11,12] Thus *de novo CACNA1A* variants may be an important and recurrent cause of severe neurodevelopmental disorders. Although *CACNA1A* LOF mutations have traditionally been associated with episodic ataxia type-2 (EA2) (OMIM: 108500)[13,14] whereas gain-of-function (GOF) mutations result in familial hemiplegic migraine-1 (FHM1) (OMIM: 141500),[15,16] the exact impact of *CACNA1A de novo* DEE-associated variants on channel function remained to be clarified.

To study the functional impact and potential pathogenicity of DEE-associated *de novo CACNA1A* variants, we expressed mutant or wild-type (WT) mouse *Cacna1a* cDNA in human embryonic kidney (HEK) 293 cells and characterized barium currents using whole-cell patch-clamp

Key Points

- We describe the clinical phenotype of four patients with severe developmental epileptic encephalopathies (DEEs) in the spectrum of Lennox-Gastaut syndrome carrying *de novo* missense variants in the *CACNA1A* gene
- We provide functional evidence demonstrating that these DEE-associated *CACNA1A de novo* mutations indeed alter $Ca_V2.1$ channel function through either a gain-of-function or a loss-of-function effect
- A better understanding of the functional impact of specific *CACNA1A* missense mutations might ultimately help guide therapies for patients with *CACNA1A*-associated DEEs

recordings. In addition, we investigated channel localization using immunocytochemical labeling in transfected HEK293 cells and in transfected mice *Cacna1a*$^{c/c}$ neurons, after deleting the endogenous allele. Finally, we predicted the impacts of the various mutations on $Ca_V2.1$ channel structure using 3D modeling. Our findings suggest that both GOF and LOF mutations can induce severe DEEs in the spectrum of LGS.

2 | METHODS

2.1 | Patient recruitment and genetic investigation

The four patients with DEE described in this study were followed at pediatric epilepsy clinics across North America. Detailed clinical history, including seizure phenotypes and neurological examination were performed by pediatric neurologists/epileptologists. Demographic, medical data, and results of laboratory and imaging studies were obtained from the medical charts. Genomic DNA was extracted from peripheral blood, and targeted gene panel sequencing, whole exome, or genome sequencing were performed in the probands, either on a research basis (Patients 2 and 4),[5,6] or through clinical testing (Baylor's, Patients 1 and 3), after obtaining informed consent from parents, as approved by medical ethics committees in each institution. Inheritance patterns were investigated by targeted sequencing in parents, and the mutations were considered to be *de novo* when not inherited, after confirming paternity status through haplotyping.

2.2 | Cloning and cDNA constructs

Full-length cDNAs encoding mouse $\alpha1_A$ (GenBank accession number AY714490), rat β3 (GenBank accession number M88751), mouse β4 (GenBank accession number BC026479.1), and rat α2/δ-1 (GenBank accession number M86621) calcium channel subunits were each cloned in the pcDNA3.1 (+)/Neo plasmid expression vector under the control of the cytomegalovirus (CMV) promoter. $Ca_V\alpha1_A$, $Ca_V\beta3$, and $Ca_V\alpha2\delta1$ plasmids (Addgene # 26578; # 26574, and # 26575, respectively[17,18]) were gifts from Diane Lipscombe. $Ca_V\beta4$ plasmid (pCMV-SPORT6, clone # 4501980) was obtained from Open Biosystems (Dharmacon Inc.). The equivalent amino acid substitutions of the following human *CACNA1A* mutations (DEE: G230V, A713T, I1357S, and V1396M; FHM1: V714A), were introduced in the mouse *Cacna1a* cDNA (DEE: G232V, A715T, I1308S, and V1347M; FHM1: V716A) by standard overlap extension PCR using specific forward and reverse primers with the overhang restriction enzyme sites HindIII, BamHI, and MauBI. All cDNA clones used in this study were sequenced in full to confirm their integrity.

2.3 | Expression in HEK293 cells and neurons

Detailed protocols are provided in Supplementary Methods. Briefly, HEK293 cells were cultured onto 12 mm glass coverslips precoated with poly-L-lysine (0.1 mg/mL each, Sigma) in 35 mm dishes and were transfected using lipofectamine 2000 (Invitrogen, CA). Plasmids expressing $Ca_V2.1$ calcium channel subunits ($\alpha1_A$ + β3 + α2/δ1), 1.6 μg/subunit, or an enhanced green fluorescent protein (EGFP) as a marker of successful transfection, were coexpressed at a molar ratio of 1:1:1:0.125 for α1A, $Ca_V\beta$, α2δ, and EGFP, using published protocols.[19–21] For selected experiments, the β4 subunit rather than the β3 subunit was coexpressed, at a molar ratio of 1:2:2:0.125 ($\alpha1_A$+β4 + α2/δ1 + EGFP).

Primary cortical neuronal cultures were prepared from *Cacna1a*$^{c/c}$ mouse postnatal cortex (P2-P4) using the Worthington Papain Dissociation System (Worthington Biochem) and protocols modified from prior publications.[22] Transfections were conducted with calcium phosphate[23] to coexpress plasmids encoding WT or mutant *Cacna1a* cDNA (1.5 μg), pCI-Cre plasmid (0.06 μg) (Promega), to delete the endogenous allele, and pIRES-EGFP (0.12 μg) (Clontech, Catalog # 6029-1) to mark transfected neurons.

Two days after transfection, HEK293 cells and neurons were processed for immunofluorescence using standard protocols (see Supplementary Methods). The following primary antibodies were used: rabbit polyclonal anti-$Ca_V\alpha1_A$ (Alomone Labs, 1:100), mouse polyclonal anti-ZO-1 (Invitrogen, 1:100), and rat polyclonal anti-GFP (Nacalai USA Inc. 1:1000). After three washes in 1XPBS, incubation with the following secondary antibodies (1:1000) was performed at room temperature for 1 hour: Alexa Fluor-488 goat anti-rat IgG, Alexa Fluor-594 goat anti-rabbit IgG, and Alexa Fluor-647 goat anti-mouse IgG (Invitrogen). Fluorescence integrated density to assess $Ca_V2.1$ channel localization was conducted using an automated detection plug-in in ImageJ (National Institutes of Health). We quantified the fluorescence integrated density within the whole cell (I_T) or the cytoplasm (I_C), after delineating the outer and inner membrane perimeter using ZO1 staining. We defined the membranous fluorescence as $I_M = (I_T - I_C)$, as described previously[24] (see Supplementary Methods).

2.4 | Electrophysiology

Whole-cell recordings were performed on EGFP$^+$ HEK293 cells with an Axopatch 700B amplifier at room temperature (19-23°C; see Supplementary Methods). Voltage-clamp recordings were low pass filtered at 2 kHz, digitized at 10 kHz using Digidata 1440A converter (Molecular Devices) and analyzed using pClamp 10 software (Molecular Devices, USA). Recordings were left to

equilibrate for 3-5 minutes after getting whole-cell access.[20] Series resistance was typically compensated by 50%-70%. The residual capacitance currents and linear leak currents were subtracted using a –*P*/4 protocol. Voltage-dependent barium currents were evoked using steps (140 msec duration) from −80 mV holding potential (Vh) to −60 to +60 mV test voltages, in 10 mV increments at 10 second intervals. Current density was obtained by dividing current amplitude by cell capacitance. For comparing mutant and WT currents, peak current density was measured during voltage steps to 0 mV. Time constant (τ) of activation was quantified on currents evoked at 10 mV fitted with the exponential equation: $Y = A_i \exp(-t/\tau) + C$. The voltage-dependence of activation was assessed from conductance (G)-voltage relationship obtained by the equation $G = I/(V_m - V_{rev})$, where V_{rev} is the extrapolated reversal potential. Activation curves were fitted by the Boltzmann equation: $G/G_{max} = 1/[1 + \exp(V-V_{0.5})/k_v]$, where $V_{0.5}$ is the potential at which the conductance is half-maximally activated, and k is the slope factor. We fitted each cell individually and obtained $V_{0.5}$ and k measures for every cell by fitting G/G_{max} curve in each cell individually, and then we calculated the mean $V_{0.5}$ and k for each group.

The following criteria were used to select cells with proper voltage clamp: series resistance was less than 15 MΩ and stable throughout the recordings; holding currents were approximately −50 pA and always less than −100 pA; currents were stable throughout the voltage-clamp recordings; and cells with peak currents less than 100 pA were excluded.[25] In addition, to minimize variability, transfections of mutant and WT channels were done at the same time and electrophysiologic recordings were interleaved on each day of experiments. We took the following precautions to minimize rundown effects on our results. First, in each experiment, we applied the protocol for current activation at 3-5 minutes after gaining whole-cell access. Second, we used the same experimental whole-cell protocols for all WT and mutant channel experiments.

2.5 | 3D structural modeling

The atomic structure of the $Ca_V1.1$ α-subunit determined by cryoelectron microscopy (PDB: 5GJV)[26] was used as a template for the generation of a homology model of mouse $Ca_V2.1$. Sequence alignments were performed using the Clustal Omega webserver.[27] Homology models were built in stages using a combination of ICM version 3.5[28] and the I-TASSER webserver.[29] Homology modeling of the transmembrane helices was performed first, to ensure fidelity to the sequence alignments, followed by a second round of model building to reintroduce the loops. Loop sampling and local minimization was performed using ICM version 3.5.[28]

2.6 | Statistics

Statistical analyses and graphs were made using SigmaPlot12.5 (Systat software) for electrophysiological data, and GraphPad Prism (v4.0; GraphPad Software) for other data. Comparisons between groups were made using one-way analysis of variance or Student's *t* test for normally distributed data; or Mann-Whitney *U* (MWU) for not normally distributed data. Data were presented as mean ± standard error of the mean (SEM), and $P < .05$ was considered statistically significant.

3 | RESULTS

3.1 | Clinical description and genetic findings

We identified four children with sporadic DEE carrying *de novo CACNA1A* missense variants (Figure 1A). The patients presented with mixed seizure disorders, global DD, moderate-severe ID, and signs of cerebellar dysfunction (ataxia, tremors) (Table 1). All variants identified were heterozygous *de novo* variants (not inherited from the parents), never reported in the ExAC (Exome Aggregation Consortium) or GAD (Genome Aggregation Database) databases.[30] The variants were located in highly conserved sequences (Figure 1B) and were predicted damaging by bioinformatics scores (SIFT, PolyphenV2) (Table 1), thus suggesting that they are likely pathogenic according to the American College of Medical Genetics and Genomics guidelines.[31] The c.2137G>A (p.A713T) variant is a known mutation, previously reported in another child with DEE.[7,11] The three other variants were novel mutations: c.4186G>A (p.V1396M), c.689G>T (p.G230V), and c.4070T>G (p.I1357S), two of which we recently reported in a study using whole genome sequencing in patients with DEE.[5] In addition, Patient 4, with the *de novo* mutation p.V1396M, also had a rare *CACNA1A* missense variant (c.6940G>A: p.G2314S) inherited from her asymptomatic mother (Figure 1A, Table 1). However, this variant was not considered pathogenic based on bioinformatics prediction tools and will not be discussed further here.

Published *CACNA1A* mutations associated with DEE, DEE with episodic ataxia (EA2), or FHM1, span most domains of the $Ca_V2.1$ channels, with a concentration of pathologic variants in the voltage-sensor segments (S4) of each domain and the intracytoplasmic loop between domains II and III of the channel, as illustrated in Figure 1C (red: *de novo* mutations in DEE; blue: inherited LOF mutations in DEE/epilepsy with EA2; yellow: inherited GOF mutations in FHM1). Three of the *CACNA1A* variants described in the current study (in Figure 1C, red lettering, red circles) are localized on the cytoplasmic side of the S4-S6 segments of the channel's transmembrane domains (S4 voltage-sensor of Domain III (p.I1357S);

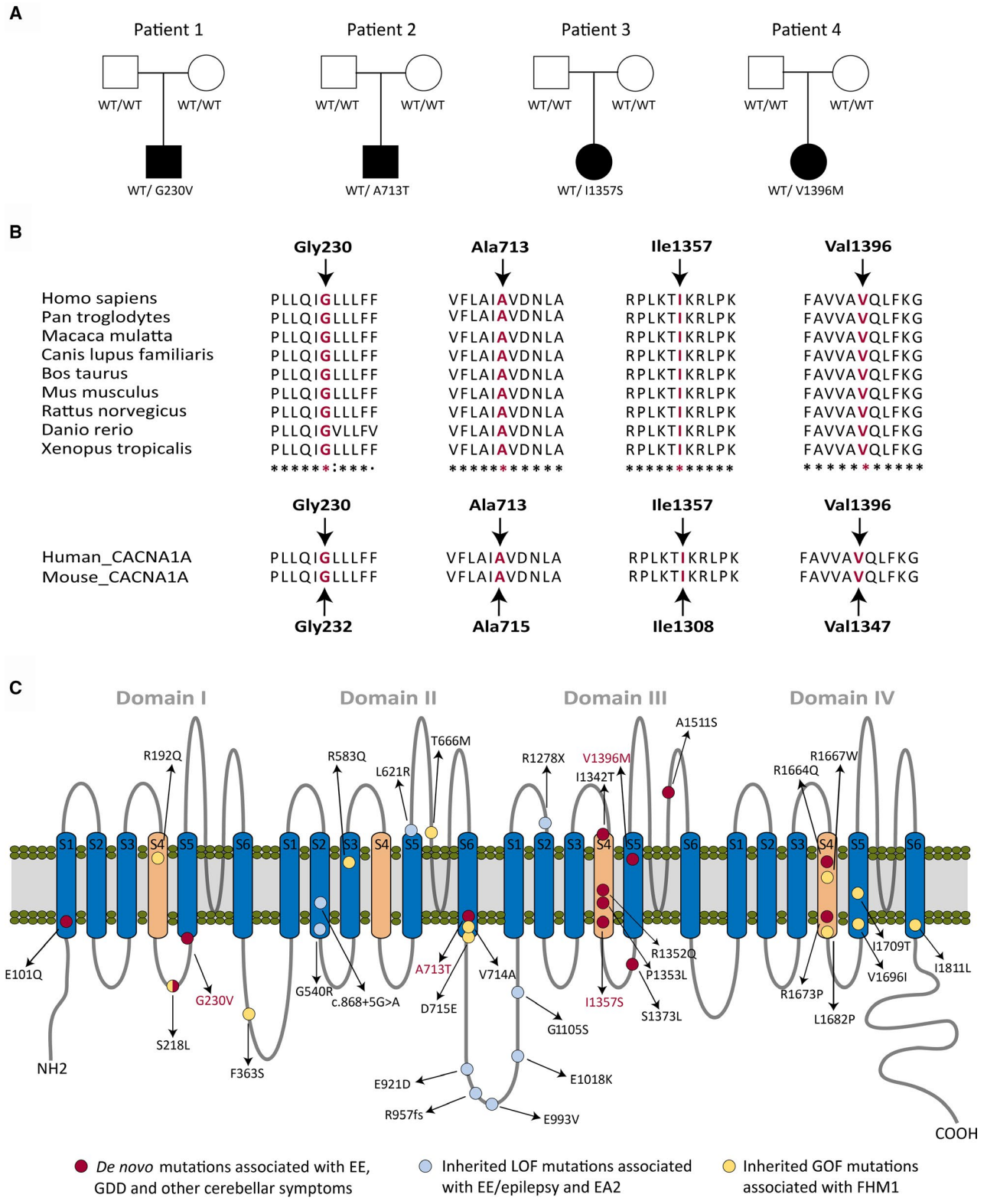

FIGURE 1 *CACNA1A* mutations. A, Pedigrees for the four affected individuals identified in this study. Note that all disorders were sporadic. B, Multiple sequence alignments of $Ca_V2.1$ alpha1 subunit protein sequences showing conservation across different species for each mutated residue. The equivalent amino acid positions in mouse *CACNA1A* are shown below. C, Schematic representation of the human $Ca_V2.1$ channel topology showing domains I-IV with transmembrane segments S1-S6. Each circle represents a mutation, color-coded as follows: EE (red; *de novo*), EA2 and EE/epilepsy (blue; inherited LOF), and FHM1 (yellow; inherited GOF). The four *de novo* mutations G230V, A713T, I1357S, and V1396M described in this study are written in red fonts

TABLE 1 Clinical characteristics of patients with de novo *CACNA1A* mutations

	Patient 1	Patient 2	Patient 3	Patient 4
Cohort	Calgary	Sainte-Justine, Montreal	Los Angeles	SickKids, Toronto
Mutation (NM_023035.2)	Exon 5: c.689G>T, p.G230V	Exon 17: c.2137G>A, p.A713T	Exon 25: c.4070T>G, p.I1357S	Exon 26: c.4186G>A, p.V1396M Exon 48: c. 6940G>A, p.G2314S
Inheritance	*De Novo*	*De Novo*	*De Novo*	*De Novo* Maternally inherited
Sequencing Approach	WES	WGS	WES	WGS
SIFT/PolyPhenV2	T/PD	D/D	D/PD	D/D, T/B
Age at onset	6 mo	2 d	<6 mo	5 mo
Gender	M	M	F	F
Syndrome	EE	LGS	EE	EE
Seizures	To, GTC, Myo, Fo status, Atyp A	GTC, Myo, At, A, To, Fo, GS	A, GTC, Myo, Febrile Sz	GTC, Fo
EEG	Gen SW	Gen or biF SW	Gen SW, diffuse slowing	R occipital slowing
DD/ID	Moderate ID	Severe ID	Severe ID	Moderate DD
Other signs/symptoms	Spasticity, hyperreflexia, mild, ataxia, tremors, alternating hemiplegia	Spasticity, hyper-reflexia, axial hypotonia, ataxia, tremors	Hypotonia, areflexia, nystagmus, ataxia, R SN hearing loss	ON glioma, limb hypotonia, hyperreflexia, ataxia, tremors
Treatment	VPA, FosPHT	PB, PHT, NTZ, VGB, RUF, VPA, TPM, LVT, CLB, CBZ,	PB, VNS, CLB, FELB, LVT, CBD, CBZ, RUF, TPM, VPA, LZP, KD	PB, LVT, PHT, P5P
MRI	Normal	Normal	Cerebellar atrophy	Normal
Reference	-	Hamdan et al. (2017)[5]	-	Hamdan et al., (2017)[5]

Abbreviation: A, absences; At, atonic; B, benign; biF, bi-frontal spike-wave discharges; CBD, cannabidiol; CBZ, carbamazepine; CLB, clobazam; D, damaging; DD, developmental delay; EE, epileptic encephalopathy unspecified; EEG, electroencephalography; F, female; FELB, felbamate; Fo, focal with secondary generalization; FosPHT, Fos-phenytoin; Gen, generalized; GS, gelastic seizures; GTC, generalized tonic-clonic; LGS, Lennox-Gastaut syndrome; ID, intellectual deficiency; KD, ketogenic diet; LVT, levetiracetam; LZP, lorazepam; M, male; Myo, myoclonic; NTZ, nitrazepam; ON, optic nerve; PB, Phenobarbital; PD, probably damaging; PHT, phenytoin; P5P, pyridoxal 5-phosphate; RUF, rufinamide; Sz, seizures; SW, spike-wave; To, tonic; T, tolerated; TPM, topiramate; VGB, vigabatrin; VNS, vagus nerve stimulator; VPA, valproic acid; WES, whole exome sequencing; WGS, whole genome sequencing.

S5 of Domain I (p.G230V), or S6 of Domain II (p.A713T)), which form the pore of the $Ca_V2.1$ channel. By contrast, the V1396M variant is positioned in the transmembrane S5 segment of Domain III, towards the extracellular milieu.

3.2 | Opposite functional impacts of DEE-associated *CACNA1A* variants on $Ca_v2.1$ channels

The effects of the *CACNA1A* variants on $Ca_v2.1$ channel function were assessed using transient expression of mouse cDNA expressing the homologous variants in HEK293 cells (Human/mouse: G230V/G232V, I1357S/I1308S, A713T/A715T, and V1396M/V1347M) followed by whole-cell recordings of voltage-gated Ba^{2+} currents. We find that the G232V and I1308S variants are LOF mutations. Indeed, the current-voltage (I-V) relation of currents from G232V or I1308S mutant (MT) channels (Figure 2A1-B1), showed a reduction in peak current density compared to WT (by 76% and 36%, respectively) (Figure 2A2-B2). Furthermore, when coexpressed with WT in a 1:1 ratio, peak current density was reduced compared to WT (by 51% for G232V and WT; 48% for I1308S and WT; Figure 2A2-B2). Similar results were obtained when we incubated the cells at 28°C or when we coexpressed the β4 instead of the β3 subunit, two established methods to increase $Ca_V2.1$ channel expression at the cell membrane[32,33] (Figure S1).

We characterized whether the coexpression of G232V or I1308S MT and WT channels affected the kinetics and voltage dependence of currents evoked at +10 mV. No difference was observed in the time constant of activation in currents of both MTs (Figure 2A2-B2). However, currents of I1308S, but not of G232V, showed a slower rate of inactivation (33%

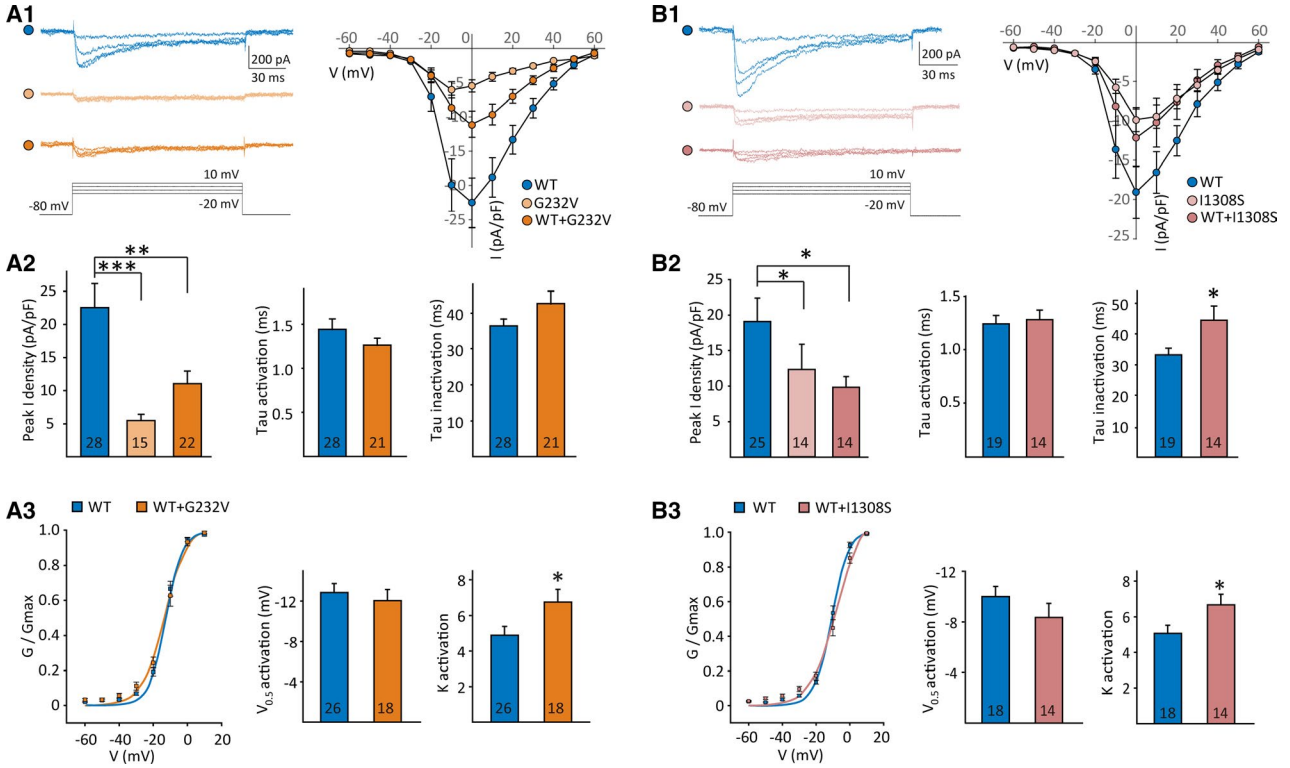

FIGURE 2 Functional effects of G232V and I1308S mutations of $Ca_V2.1$ channels. A1, (left) Representative whole-cell voltage-clamp recordings of barium currents in HEK293 cells expressing WT (top), G232V mutant (middle), and combination of WT+ G232V (1:1 ratio) (bottom) $Ca_V2.1$ channels, obtained by voltage steps shown below. (right) Plots of current density-voltage relations for WT, G232V and WT+ G232V mutant currents for all cells. A2, The isomolar coexpression of the G232V MT channel with the WT channel reduces peak current density compared to that of the WT channel alone. Summary graphs of peak current density (at 0 mV) for WT (blue), G232V (pale orange), and WT+ G232V currents (orange) (left), time constant of activation (middle) and inactivation (right) for WT (blue) and WT+ G232V currents (orange). A3, The G232V variants reduce the slope of the activation curve. (left) Plots of activation curves for WT (blue) and WT+ G232V currents (orange). Solid lines are Boltzmann equation fit. Summary graphs for all cells of midactivation point ($V_{0.5}$ activation) (middle) and slope factor of activation curves (k activation) (right) B1-B3, Similar representations for WT (blue), 1308S (pale pink), and combination of WT+ I1308S (pink) (1:1) mutant currents. Numbers in bar graphs represent number of cells. $*P < .05$, $**P < .01$, $***P < .001$, compared to WT (MWU test for non normal data or Student's *t* test for normally distributed data)

increase in time constant). Furthermore, we observed a decreased slope of the activation curve for both the G232V MT and I1308S MT (Figure 2A3,B3). Thus G232V or I1308S mutant currents are less activated by voltage. However, these subtle changes are unlikely to account for the large reduction in peak current density, which might reflect reduced channel expression at the cell surface.

In contrast, cells expressing A715T MT channels displayed a GOF effect. The I-V relation of A715T MT currents showed larger peak current density (89% increase; Figure 3A1-A2) relative to WT, as observed for the known FHM1-associated GOF mutation (mouse V716A; human V714A)[34] (91% increase; Figure 3B1-B2). However, relative to the V716A variant, the A715T variant induced changes in current kinetics with slower current inactivation (252% increase; Figure 3A2) and a leftward shift of the activation curve, with a steeper slope and a more hyperpolarized midpoint of activation (changed by −10 mV; Figure 3A3). V716A MT currents showed only a steeper slope of the activation curve compared to WT (Figure 3B3). These results suggest that the A715T mutation results in a GOF of $Ca_V2.1$ channels with a combination of larger currents and negative shift in voltage dependence of activation with an impact greater than that of the FHM1- V716A variant, which does not significantly affect current kinetics.

With the same paradigm, the V1347M MT channels displayed similar peak currents, I-V relation, kinetics, and voltage dependence as WT currents (Figure 3C1-C3). However, using different subunit ratios and accessory subunits to enhance membrane expression (1:2:2 ratio of α1a: β4: α2δ),[35] the V1347M variant induced a GOF of $Ca_V2.1$ channels. I-V relation of V1347M MT currents showed larger peak current density (49% increase; Figure 3D1-D2) relative to WT. Kinetics of V1347M MT currents were unchanged (Figure 3D2) but voltage dependence of activation was altered. The slope of the activation curve was steeper and the midpoint of activation was more hyperpolarized (shifted by −5 mV; Figure 3D3). These findings suggest that the

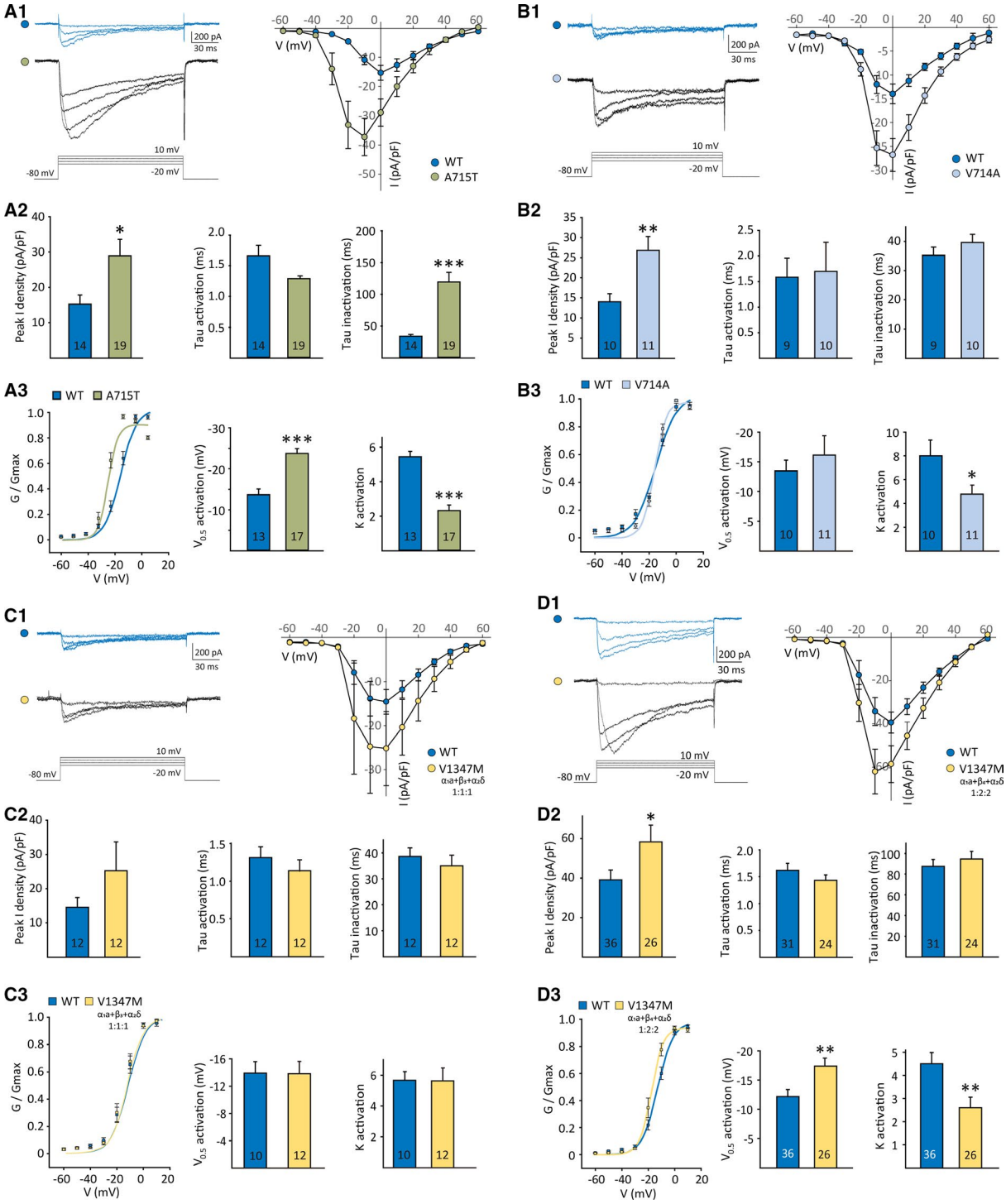

FIGURE 3 Functional effects of the A715T, V716A, and V1347M mutations of $Ca_V2.1$ channel. A1, (left) Representative whole-cell voltage-clamp recordings of barium currents in HEK293 cells expressing WT (top) and A715T (bottom) $Ca_V2.1$ channels, obtained by voltage steps, as shown below (right). Plots of current density-voltage relations for WT and A715T mutant currents for all cells. A2, A715T mutation increased current density and affected current kinetics. Summary graphs for all cells of peak current density (at 0 mV) for WT and A715T currents (left), time constant of activation (middle), and inactivation (right) for WT (blue) and A715T (green) currents. A3, The A715T mutation induces a leftward shift in the voltage dependence of activation. (left) Plots of activation curves for WT (blue) and A715T (green) currents. Solid lines are Boltzmann equation fit. Summary graphs for all cells of mid-activation point ($V_{0.5}$ activation) (middle) and slope factor of activation curves (k activation) (right). B1-B3, Similar representation for WT (blue) and V716A mutant currents (pale blue). C and D, Similar representation for WT (blue) and V1347M mutant currents (yellow), by cotransfecting subunits with the following ratio: α1a + β3 + α2/δ (1:1:1) (C1-C3) and α1a + β4 + α2/δ (1:2:2) (D1-D3). Numbers in bar graphs represent number of cells. *$P < .05$, **$P < .01$, ***$P < .001$, compared to WT (MWU test for nonnormal data or Student's *t* test for normally distributed data)

V1347M mutation causes a GOF effect with larger currents and a more pronounced voltage dependence of activation.

Taken together, our results indicate that the G232V and I1308S mutations exert an LOF effect, whereas the A715T and V1347M mutations induce a GOF effect on $Ca_V2.1$ channels. In addition, the A715T and V1347M mutations appear to facilitate current activation.

3.3 | Cell surface expression of $Ca_V2.1$ mutant channels

To assess whether the mutations reported here also affect the channel localization at the cell membrane, we performed immunocytochemical staining after 48 hours of transfection for $Ca_V2.1$ and a cellular membrane marker (ZO-1) in HEK293 cells transfected with the WT or MT *Cacna1a* cDNAs and associated β3 and α2δ-1 subunits (as above). Although the A715T MT channels are properly expressed at the cell membrane, similar to WT channels, the G232V and I1308S MT channels accumulate in intracytoplasmic inclusions, with minimal membranous expression (Figure 4A). The V1347M MT channels display an intermediate phenotype with a 50% reduction of membranous expression compared to WT (Figure 4A).

Given that channel subunit trafficking to the cell membrane may differ in neurons due to the availability of native binding partners and associated subunits, we next sought to

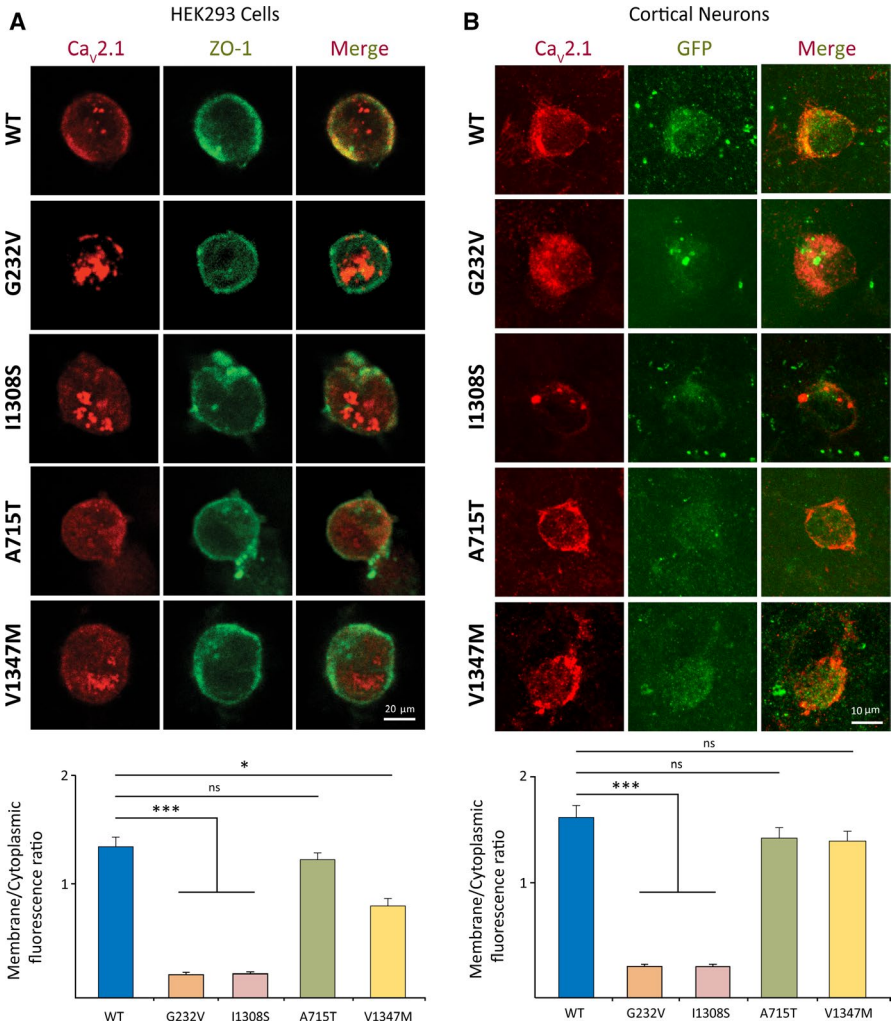

FIGURE 4 Impact of various mutations on $Ca_V2.1$ channels expression. A, Representative examples of $Ca_V2.1$ channel localization revealed by immunostaining for the α1 subunit of $Ca_V2.1$ (red) and the cell membrane protein ZO-1 (green) in HEK293 cells. Note the significant intracytoplasmic accumulation for LOF mutant channels (G232V, I1308S) and intermediate phenotype for the GOF V1347M mutant channels. The graph shows quantification of fluorescence intensity indicating significantly reduced membrane expression relative to cytoplasmic expression for $Ca_V2.1$ G232V (pale orange) and I1308S (pale pink) mutant channels compared to WT (blue), and intermediate phenotype for V1347M (yellow) mutant channels ($n \geq 40$ cells per genotype). B, Representative examples of $Ca_V2.1$ channel localization revealed by immunostaining for the α1 subunit of $Ca_V2.1$ (red) and GFP (green), were quantification illustrated in the graph below ($n \geq 40$ neurons per genotype). $^*P < .05$, $^{***}P < .001$, ns: nonsignificative by one-way analysis of variance (ANOVA) with Dunnett's multiple comparisons test. Error bars represent means ± standard error of the mean (SEM)

assess whether the deficits in channel trafficking observed in HEK293 cells also occurred in neurons. We thus expressed the WT or MT cDNA in primary neurons derived from mice carrying a conditional *Cacna1a* allele and deleted the endogenous allele by coexpressing the Cre recombinase. We observed similar deficits in channel intracellular trafficking for the G232V and I1308S MT channels, with clustering of the MT protein in intracytoplasmic inclusions (Figure 4B). By contrast, both the A715T and V1347M MTs were properly expressed at the cell membrane, with levels comparable to those of the WT channels (Figure 4B).

3.4 | Impact of *de novo CACNA1A* mutations on $Ca_V2.1$ structure

To predict the functional impact of the mutations reported here on $Ca_V2.1$ channel structure, we generated a homology model based on the atomic resolution structure of $Ca_V1.1$ channels (Figure 5A,B). Modeling of the A715T MT channels suggests that the presence of a threonine in this position distorts the helix, thus inducing steric clashes with the F365 residue (Figure 5C, left), which do not occur in the WT channels. This highly constrained conformation is energetically unfavorable. Relieving this strain could induce a conformational change that favors channel opening thereby leading to a GOF phenotype. Similarly, modeling of the V1347M mutation suggests that the novel methionine residue induces a steric clash with neighboring residues (V506, V1344, and V1399) that does not occur in WT channels (Figure 5C, right). We postulate that these steric clashes prevent the motion of the voltage-sensor domain downward toward its resting state, rendering the channels more sensitive to depolarization and increasing channel open time.

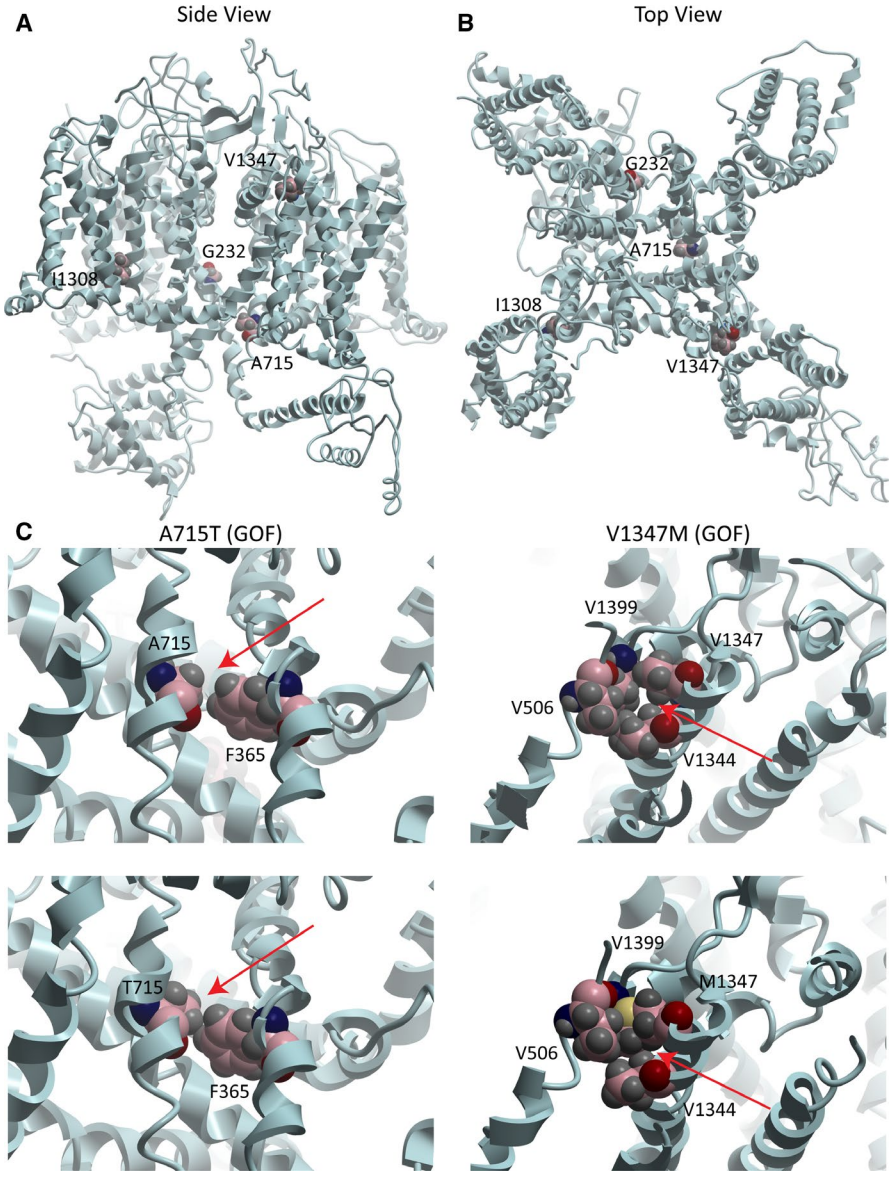

FIGURE 5 3D structure of the $Ca_V2.1$ channels using in silico modeling. A, Side view; B, Axial view. Color dots illustrate the position of individual mutations represented here in the mouse $Ca_V2.1$ channel. C, Both GOF mutations (A715T and V1347M) are predicted to induce steric clashes with nearby residues on adjacent loops, thus altering channel gating

By contrast, no obvious conformational changes were observed for the two LOF variants G232V and I1308S (data not shown). Thus, although GOF mutations exert their effect at least partly through structural changes that prevent proper gating of $Ca_V2.1$ channels, the two LOF mutations likely exert their effect by preventing proper channel trafficking to the cell membrane. Alternatively, these mutations may exert their effects in other conformational states not represented in the atomic structure.

4 | DISCUSSION

Here, we report four patients with *de novo* missense mutations in the *CACNA1A* gene presenting with a developmental phenotype characterized by DEE with severe refractory seizures starting in the first 6 months of life, global developmental delay evolving toward moderate to severe ID, and variable motor symptoms (ataxia, tremors, spasticity, alternating hemiplegia). Whereas LOF mutations in *CACNA1A* have been associated traditionally with EA2,[14] GOF mutations have been associated with FHM1.[15] We recently found that inherited *CACNA1A* LOF mutations cause EE with cognitive impairment, autism, and a mild EA2 phenotype,[10] and that *de novo* missense *CACNA1A* variants can be found in 1% of children with a more severe EE in the spectrum of Lennox-Gastaut syndrome,[5] as described also by others.[11] However, the mechanisms by which some *de novo* missense variants cause such a profound phenotype were unclear. We now show that both LOF (G230V, I1357S) and GOF (A713T, V1396M) missense mutations cause severe DEE, with additional impacts of GOF mutations on current activation and inactivation properties not seen with previously reported FHM1-associated GOF mutations.

Furthermore, the LOF mutations described here resulted in reduced channel trafficking to the cell membrane, with clustering in intracytoplasmic inclusions, whereas the coexpression of the MT and WT cDNA reduced the peak current density by half compared to that of WT channels. Together, these data suggest the possibility of a dominant-negative effect by which the MT subunit prevents the proper shuttling of the WT channel to the cell membrane, as described for other EA2-associated *CACNA1A* mutations causing protein misfolding and pathologic interactions between MT and WT subunits with sequestration in the endoplasmic reticulum.[36,37] Although this possibility should be explored further, a dominant-negative effect would be consistent with the more severe phenotype observed in patients with *de novo* LOF mutations (G230V and I1357S) compared to patients with hereditary heterozygous haploinsufficiency (ie, gene deletion, frameshift, or stop-gain mutations).[10]

Of interest, different *CACNA1A* GOF and LOF mutations have also been recently associated with developmental ataxia, global developmental delay, and progressive cerebellar atrophy in children,[12] suggesting that *CACNA1A* mutations with opposite functional impact can have similar severe developmental presentations. Furthermore, both GOF or LOF mutations in other neuronal channels have been associated with DEE of variable severity (*SCN1A*,[38] *KCNQ2*,[39] *KCNQ5*,[40] *KCNA2*[41] and *KCNB1*[42]).

The mechanisms by which GOF or LOF mutations can both result in similar epilepsy phenotypes may lie in the differential impact of such mutations in different component of neuronal circuits. For *CACNA1A*, we previously demonstrated that, in $Nkx2.1^{Cre}$; $Cacna1a^{c/c}$ mice, LOF of *Cacna1a* in cortical and hippocampal GABAergic interneurons selectively impairs synaptic release from parvalbumin-positive fast-spiking basket cells, whereas somatostatin-positive INs are unaffected, and that this is sufficient to cause epilepsy.[43] By contrast, the deletion of *Cacna1a* in all cortical pyramidal cells ($Emx1^{Cre}$; $Cacna1a^{c/c}$ mice) did not result in epilepsy in early adulthood, although it did reduce cortical excitability and alleviated the seizure phenotype in double-mutant mice ($Nkx2.1^{Cre}$; $Emx1^{Cre}$; $Cacna1a^{c/c}$ mice).[43] In addition, circuit remodeling with a gain of thalamic excitability results in later-onset epilepsy when *Cacna1a* is deleted selectively in layer VI pyramidal cells.[44] Thus in the case of *Cacna1a* LOF mutation, a primary impairment of GABA release from cortical and limbic interneurons is predicted to drive seizure onset.

The mechanisms by which some *CACNA1A* GOF mutations result in epilepsy remain to be explored but likely reflect the functional impact of the particular variants on channel function. Indeed, although most patients with FHM1 carrying GOF *CACNA1A* mutations do not develop seizures (ie, R192Q[45]), a minority of patients develop complex phenotypes with hemiplegic migraine, ataxia, and transient posttraumatic brain edema with seizures, presumably due to the greater impact of specific variants on peak current density (ie, S218L).[46,47] Furthermore, although heterozygous knockin mice for the R192Q and S218L mutations do not develop seizures, homozygous mutants for the S218L variant develop epilepsy, likely reflecting gene dosage effects.[48] Thus GOF variants that induce greater impacts than the FHM1-associated variants on calcium currents have a higher likelihood of inducing epilepsy. We find that, in contrast to the FHM1-associated V714A mutation, both EE-associated GOF mutations identified here (A713T, V1396M) also perturb current kinetics (shift of activation toward more hyperpolarized potentials) resulting in an even greater impact on net charge transfer with prolonged currents, suggesting that the magnitude of the functional impact on $Ca_V2.1$ currents determines the clinical phenotype.

Nonetheless, the network mechanisms by which some GOF variants cause epilepsy while others do not remain to be explored. Although the FHM1-associated GOF mutations result in facilitated glutamatergic transmission at

pyramidal cell synapses with unaltered inhibitory transmission from GABAergic interneurons (see *Cacna1a*^{R192Q} *and* *Cacna1a*^{S218L} mice[49]), it is possible that DEE-associated variants that induce much greater GOF due to combined gain of conductance and channel open time might indirectly affect other components of the neuronal networks, perhaps through calcium excitotoxicity and cell death. This will need to be explored further using appropriate animal models.

Finally, given that both LOF and GOF *CACNA1A* mutations present with similarly severe DEE phenotypes, functional validation is essential to correctly attribute pathogenicity and to clarify the molecular mechanisms by which novel variants affect $Ca_V2.1$ channels. Future clinical characterization of larger patient cohorts together with functional validation of individual mutations may help distinguish clinical endophenotypes associated with LOF or GOF mutations. In turn, this may help guide future therapies, since patients with GOF mutations might be predicted to respond to $Ca_V2.1$ antagonists, whereas patients carrying dominant-negative LOF mutations might respond to peptide inhibitors or chaperones designed to enhance trafficking of the channels to the cell membrane.[50] Ultimately, clarifying the mechanisms by which specific mutations affect the function and localization of $Ca_V2.1$ channels will improve therapeutic interventions for patients with *CACNA1A*-associated DEEs.

ACKNOWLEDGMENTS

We thank the families involved in this project for their dedication and collaboration. This work was supported by grants from the Savoy Foundation, Epilepsy Canada Foundation, RMGA, and CIHR, to E.R; as well as by CIHR and FRQS, GRSNC (Group grant) to J-C.L. E. R. receives a clinician-scientist salary award from FRQS and a Young Investigator Award from the CIHR. J-C.L. is the recipient of the Canada Research Chair in Cellular and Molecular Neurophysiology. X. J. received a postdoctoral training award from the Savoy Foundation. T.M.P. was funded by the Cedars-Sinai institutional funding and the Cedars-Sinai Diana and Steve Marienhoff Fashion Industries Guild Endowed Fellowship in Pediatric Neuromuscular Diseases.

CONFLICT OF INTEREST

The authors have no conflict of interest to disclose. We confirm that we have read the Journal's position on issues involved in ethical publication and declare that this report is consistent with those guidelines.

ORCID

Jean-Claude Lacaille https://orcid.org/0000-0003-4056-0574

Elsa Rossignol https://orcid.org/0000-0002-9304-9385

REFERENCES

1. Berg AT, Berkovic SF, Brodie MJ, Buchhalter J, Cross JH, van Emde Boas W, et al. Revised terminology and concepts for organization of seizures and epilepsies: report of the ILAE Commission on Classification and Terminology, 2005-2009. Epilepsia. 2010;51:676–85.
2. Nabbout R, Epilepsy Dulac O. Genetics of early-onset epilepsy with encephalopathy. Nat Rev Neurol. 2012;8:129–30.
3. Covanis A. Clinical management of epileptic encephalopathies of childhood and infancy. Expert Rev Neurother. 2014;14:687–701.
4. Allen NM, Conroy J, Shahwan A, Lynch B, Correa RG, Pena SD, et al. Unexplained early onset epileptic encephalopathy: exome screening and phenotype expansion. Epilepsia. 2016;57:e12–7.
5. Hamdan FF, Myers CT, Cossette P, Lemay P, Spiegelman D, Laporte AD, et al. High rate of recurrent *de novo* mutations in developmental and epileptic encephalopathies. Am J Hum Genet. 2017;101:664–85.
6. Michaud JL, Lachance M, Hamdan FF, Carmant L, Lortie A, Diadori P, et al. The genetic landscape of infantile spasms. Hum Mol Genet. 2014;23:4846–58.
7. Epi4K Consortium, Epilepsy Phenome/Genome Project; Allen AS, Berkovic SF, Cossette P, Delanty N, et al. *De novo* mutations in epileptic encephalopathies. Nature. 2013;501:217–21.
8. Mei D, Parrini E, Marini C, Guerrini R. The impact of next-generation sequencing on the diagnosis and treatment of epilepsy in paediatric patients. Mol Diagn Ther. 2017;21:357–73.
9. Veeramah KR, Johnstone L, Karafet TM, Wolf D, Sprissler R, Salogiannis J, et al. Exome sequencing reveals new causal mutations in children with epileptic encephalopathies. Epilepsia. 2013;54:1270–81.
10. Damaj L, Lupien-Meilleur A, Lortie A, Riou E, Ospina LH, Gagnon L, et al. CACNA1A haploinsufficiency causes cognitive impairment, autism and epileptic encephalopathy with mild cerebellar symptoms. Eur J Hum Genet. 2015;23:1505–12.
11. Epi KC. *De novo* mutations in *SLC1A2* and *CACNA1A* are important causes of epileptic encephalopathies. Am J Hum Genet. 2016;99:287–98.
12. Travaglini L, Nardella M, Bellacchio E, D'Amico A, Capuano A, Frusciante R, et al. Missense mutations of *CACNA1A* are a frequent cause of autosomal dominant nonprogressive congenital ataxia. Eur J Paediatr Neurol. 2017;21:450–6.
13. Mantuano E, Romano S, Veneziano L, Gellera C, Castellotti B, Caimi S, et al. Identification of novel and recurrent *CACNA1A* gene mutations in fifteen patients with episodic ataxia type 2. J Neurol Sci. 2010;291:30–6.
14. Rajakulendran S, Graves TD, Labrum RW, Kotzadimitriou D, Eunson L, Davis MB, et al. Genetic and functional characterisation of the P/Q calcium channel in episodic ataxia with epilepsy. J Physiol. 2010;588:1905–13.
15. Pietrobon D. Insights into migraine mechanisms and $Ca_V2.1$ calcium channel function from mouse models of familial hemiplegic migraine. J Physiol. 2010;588:1871–8.
16. Kors EE, Haan J, Giffin NJ, Pazdera L, Schnittger C, Lennox GG, et al. Expanding the phenotypic spectrum of the *CACNA1A* gene

T666M mutation: a description of 5 families with familial hemiplegic migraine. Arch Neurol. 2003;60:684–8.
17. Richards KS, Swensen AM, Lipscombe D, Bommert K. Novel $Ca_V2.1$ clone replicates many properties of Purkinje cell $Ca_V2.1$ current. Eur J Neurosci. 2007;26:2950–61.
18. Lin Y, McDonough SI, Lipscombe D. Alternative splicing in the voltage-sensing region of N-Type $Ca_V2.2$ channels modulates channel kinetics. J Neurophysiol. 2004;92:2820–30.
19. Garza-Lopez E, Sandoval A, Gonzalez-Ramirez R, Gandini MA, Van den Maagdenberg A, De Waard M, et al. Familial hemiplegic migraine type 1 mutations W1684R and V1696I alter G protein-mediated regulation of Ca(V)2.1 voltage-gated calcium channels. Biochim Biophys Acta. 1822, 2012,;1238–46.
20. Garza-Lopez E, Gonzalez-Ramirez R, Gandini MA, Sandoval A, Felix R. The familial hemiplegic migraine type 1 mutation K1336E affects direct G protein-mediated regulation of neuronal P/Q-type Ca2 + channels. Cephalalgia. 2013;33:398–407.
21. Gandini MA, Sandoval A, Felix R. Whole-cell patch-clamp recording of recombinant voltage-sensitive Ca2 + channels heterologously expressed in HEK-293 cells. Cold Spring Harb Protoc. 2014;2014:396–401.
22. Huettner JE, Baughman RW. Primary culture of identified neurons from the visual cortex of postnatal rats. J Neurosci. 1986;6:3044–60.
23. Audet N, Charfi I, Mnie-Filali O, Amraei M, Chabot-Doré AJ, Millecamps M, et al. Differential association of receptor-Gbetagamma complexes with beta-arrestin2 determines recycling bias and potential for tolerance of delta opioid receptor agonists. J Neurosci. 2012;32:4827–40.
24. Jeng CJ, Sun MC, Chen YW, Tang CY. Dominant-negative effects of episodic ataxia type 2 mutations involve disruption of membrane trafficking of human P/Q-type Ca2 + channels. J Cell Physiol. 2008;214:422–33.
25. Spacey SD, Hildebrand ME, Materek LA, Bird TD, Snutch TP. Functional implications of a novel EA2 mutation in the P/Q-type calcium channel. Ann Neurol. 2004;56:213–20.
26. Wu J, Yan Z, Li Z, Qian X, Lu S, Dong M, et al. Structure of the voltage-gated calcium channel Ca(v)1.1 at 3.6 A resolution. Nature. 2016;537:191–6.
27. Sievers F, Higgins DG. Clustal omega. Curr Protoc Bioinformatics. 2014;48: 3 13 11–6.
28. Abagyan R, Totrov M, Kuznetsov D. ICM—A new method for protein modeling and design: applications to docking and structure prediction from the distorted native conformation. J Comput Chem. 1994;15:488–506.
29. Yang J, Yan R, Roy A, Xu D, Poisson J, Zhang Y. The I-TASSER Suite: protein structure and function prediction. Nat Methods. 2015;12:7–8.
30. Lek M, Karczewski KJ, Minikel EV, Samocha KE, Banks E, Fennell T, et al. Analysis of protein-coding genetic variation in 60,706 humans. Nature. 2016;536:285–91.
31. Richards S, Aziz N, Bale S, Bick D, Das S, Gastier-Foster J, et al. Standards and guidelines for the interpretation of sequence variants: a joint consensus recommendation of the American College of Medical Genetics and Genomics and the Association for Molecular Pathology. Genet Med. 2015;17:405–24.
32. Mich PM, Horne WA. Alternative splicing of the Ca2 + channel beta4 subunit confers specificity for gabapentin inhibition of Cav2.1 trafficking. Mol Pharmacol. 2008;74:904–12.
33. Terragni B, Scalmani P, Franceschetti S, Cestèle S, Mantegazza M. Post-translational dysfunctions in channelopathies of the nervous system. Neuropharmacology. 2018;132:31–42.
34. Hans M, Luvisetto S, Williams ME, Spagnolo M, Urrutia A, Tottene A, et al. Functional consequences of mutations in the human alpha1A calcium channel subunit linked to familial hemiplegic migraine. J Neurosci. 1999;19:1610–9.
35. Dolphin AC. Beta subunits of voltage-gated calcium channels. J Bioenerg Biomembr. 2003;35:599–620.
36. Page KM, Heblich F, Davies A, Butcher AJ, Leroy J, Bertaso F, et al. Dominant-negative calcium channel suppression by truncated constructs involves a kinase implicated in the unfolded protein response. J Neurosci. 2004;24:5400–9.
37. Dahimene S, Page KM, Nieto-Rostro M, Pratt WS, D'Arco M, Dolphin AC. A $Ca_V2.1$ N-terminal fragment relieves the dominant-negative inhibition by an episodic ataxia 2 mutant. Neurobiol Dis. 2016;93:243–56.
38. Schutte SS, Schutte RJ, Barragan EV, O'Dowd DK. Model systems for studying cellular mechanisms of *SCN1A*-related epilepsy. J Neurophysiol. 2016;115:1755–66.
39. Orhan G, Bock M, Schepers D, Ilina EI, Reichel SN, Löffler H, et al. Dominant-negative effects of *KCNQ2* mutations are associated with epileptic encephalopathy. Ann Neurol. 2014;75:382–94.
40. Lehman A, Thouta S, Mancini GMS, Naidu S, van Slegtenhorst M, McWalter K, et al. Loss-of-function and gain-of-function mutations in *KCNQ5* cause intellectual disability or epileptic encephalopathy. Am J Hum Genet. 2017;101:65–74.
41. Syrbe S, Hedrich UBS, Riesch E, Djémié T, Müller S, Møller RS, et al. *De novo* loss- or gain-of-function mutations in *KCNA2* cause epileptic encephalopathy. Nat Genet. 2015;47:393–9.
42. Torkamani A, Bersell K, Jorge BS, Bjork RL Jr, Friedman JR, Bloss CS, et al. *De novo KCNB1* mutations in epileptic encephalopathy. Ann Neurol. 2014;76:529–40.
43. Rossignol E, Kruglikov I, van den Maagdenberg AM, Rudy B, Fishell G. Ca_V 2.1 ablation in cortical interneurons selectively impairs fast-spiking basket cells and causes generalized seizures. Ann Neurol. 2013;74:209–22.
44. Bomben VC, Aiba I, Qian J, Mark MD, Herlitze S, Noebels JL. Isolated P/Q calcium channel deletion in layer VI corticothalamic neurons generates absence epilepsy. J Neurosci. 2016;36: 405–18.
45. Ophoff RA, Terwindt GM, Vergouwe MN, van Eijk R, Oefner PJ, Hoffman SM, et al. Familial hemiplegic migraine and episodic ataxia type-2 are caused by mutations in the Ca2 + channel gene *CACNL1A4*. Cell. 1996;87:543–52.
46. Chan YC, Burgunder JM, Wilder-Smith E, Chew SE, Lam-Mok-Sing KM, Sharma V, et al. Electroencephalographic changes and seizures in familial hemiplegic migraine patients with the *CACNA1A* gene S218L mutation. J Clin Neurosci. 2008;15:891–4.
47. Stam AH, Luijckx GJ, Poll-The BT, Ginjaar IB, Frants RR, Haan J, et al. Early seizures and cerebral oedema after trivial head trauma associated with the *CACNA1A* S218L mutation. J Neurol Neurosurg Psychiatry. 2009;80:1125–9.
48. van den Maagdenberg AM, Pizzorusso T, Kaja S, Terpolilli N, Shapovalova M, Hoebeek FE, et al. High cortical spreading depression susceptibility and migraine-associated symptoms in Ca(v)2.1 S218L mice. Ann Neurol. 2010;67:85–98.
49. Di Guilmi MN, Wang T, Inchauspe CG, Forsythe ID, Ferrari MD, van den Maagdenberg AM, et al. Synaptic gain-of-function effects

of mutant Cav2.1 channels in a mouse model of familial hemiplegic migraine are due to increased basal [Ca2 +]i. J Neurosci. 2014;34:7047–58.

50. Bechi G, Rusconi R, Cestele S, Franceschetti S, Mantegazza M. Rescuable folding defective $Na_V1.1$ (*SCN1A*) mutants in epilepsy: properties, occurrence, and novel rescuing strategy with peptides targeted to the endoplasmic reticulum. Neurobiol Dis. 2015;75:100–14.

SUPPORTING INFORMATION

Additional supporting information may be found online in the Supporting Information section at the end of the article.

How to cite this article: Jiang X, Raju PK, D'Avanzo N, et al. Both gain-of-function and loss-of-function *de novo CACNA1A* mutations cause severe developmental epileptic encephalopathies in the spectrum of Lennox-Gastaut syndrome. *Epilepsia*. 2019;60:1881–1894. https://doi.org/10.1111/epi.16316